Climate Dynamics (2004) 23: 117–132
DOI 10.1007/s00382-004-0426-9

K. W. Oleson · G. B. Bonan · S. Levis · M. Vertenstein

Effects of land use change on North American climate: impact of surface datasets and model biogeophysics

Received: 2 July 2003 / Accepted: 8 March 2004 / Published online: 19 May 2004

Abstract This study examines the impact of historical land-cover change on North American surface climate, focusing on the robustness of the climate signal with respect to representation of sub-grid heterogeneity and land biogeophysics within a climate model. We performed four paired climate simulations with the Community Atmosphere Model using two contrasting land models and two different representations of land-cover change. One representation used a biome classification without subgrid-scale heterogeneity while the other used high-resolution satellite data to prescribe multiple vegetation types within a grid cell. Present-day and natural vegetation datasets were created for both representations. All four sets of climate simulations showed that present-day vegetation has cooled the summer climate in regions of North America compared to natural vegetation. The simulated magnitude and spatial extent of summer cooling due to land-cover change was reduced when the biome-derived land-cover change datasets were replaced by the satellite-derived datasets. The diminished cooling is partly due to reduced intensity of agriculture in the satellite-derived datasets. Comparison of the two land-surface models showed that the use of a comparatively warmer and drier land model in conjunction with satellite-derived datasets further reduced the simulated magnitude of summer cooling. These results suggest that the cooling signal associated with North American land-cover change is robust but the magnitude and therefore detection of the signal depends on the realism of the datasets used to represent land-cover change and the parametrisation of land biogeophysics.

K. W. Oleson (✉) · G. B. Bonan · S. Levis · M. Vertenstein
Climate and Global Dynamics Division,
National Center for Atmospheric Research,
PO Box 3000, Boulder, CO 80307-3000, USA
E-mail: oleson@ucar.edu

1 Introduction

Much of the natural needleleaf evergreen and broadleaf deciduous forests of the eastern USA and to a lesser extent the grasslands of the central USA have been converted to agriculture. Several modeling studies have shown that this land-cover change results in a cooling in surface climate (Matthews et al. 2003; Bounoua et al. 2002; Govindasamy et al. 2001; Betts 2001; Bonan 1997, 1999; Brovkin et al. 1999; Hansen et al. 1998). In particular, Bonan (1997, 1999) concluded that modern vegetation causes cooling in daily mean temperature over the central USA in summer as well as a reduction in the diurnal temperature range. Bonan (2001) analyzed geographic patterns in station temperature records in relation to land-cover and appeared to find a temperature signal that supported the model studies. However, the temperature signal associated with this land use is small and is difficult to demonstrate in light of natural climate variability and larger climate forcings such as greenhouse gases and aerosols.

Another approach to gain confidence in the climate model simulations is to demonstrate the robustness of the land-use signal. One possible deficiency in previous studies is representation of land-cover and landscape heterogeneity. For example, the surface datasets used by Bonan (1997, 1999) were derived from a biome classification map. A grid cell could only be classified as a single land-cover type, and consequently, fine-scale heterogeneity in land-cover, especially croplands, was not represented. The advent of 1-km satellite-derived land-cover datasets and their inclusion in climate models (e.g., Bonan et al. 2002a,b) allows a much more realistic depiction of the land surface. In addition, though all land-surface models simulate common processes such as energy, moisture, and momentum exchange with the atmosphere and the associated hydrologic cycle, they differ greatly in their parametrisation of these processes.

Here, we conduct climate model simulations to examine uncertainty in the land-use forcing of climate associated with surface datasets and model parametrisations. The climate simulations use the Community Atmosphere Model (CAM2) with two different land-surface models and two different surface datasets. The land-surface models are the NCAR land-surface Model (LSM1) and the Community Land Model (CLM2). Each model is configured to use two types of surface data: (a) a biome classification without subgrid-scale heterogeneity; and (b) a satellite-based dataset with multiple vegetation types in a grid cell. Both types of surface data are configured for present-day and natural vegetation in the USA to estimate the land-use forcing of climate.

2 Methods

2.1 Land model descriptions

The National Center for Atmospheric Research (NCAR) Land Surface Model (LSM version 1) is the land-surface parametrisation used with the NCAR Community Climate Model and the NCAR Climate System Model (Bonan 1996, 1998). The land model has been significantly revised as part of the development of the next version of these climate models. The new model is known as the Community Land Model (CLM2) (Bonan et al. 2002a).

2.1.1 Biogeophysics

CLM2's biogeophysical parametrisations differ significantly from LSM1. CLM2 has ten layers for soil temperature and soil water with explicit treatment of liquid water and ice, while LSM1 has six layers with an apparent heat capacity that accounts for phase change. CLM2 uses a multi-layer snow with heat and water flow between snow layers. LSM uses a one-layer snow mass balance blended with the top soil layer for heat transfer. Both models use Monin-Obukhov similarity theory but with different flux gradient relations and aerodynamic resistance formulations. Parametrisations for surface runoff and base flow are significantly different with runoff in CLM2 based on a TOPMODEL-like approach (Beven and Kirkby 1979). A detailed description of differences between CLM2 and LSM1 can be found in Bonan et al. (2002a). Simulations with CLM2 show significant improvements in surface air temperature, snow cover, and runoff in some regions compared to LSM1 (Bonan et al. 2002a).

In general, CLM2 is a drier, warmer model than LSM1 (Bonan et al. 2002a). CLM2 has higher canopy interception of precipitation and higher surface runoff, which results in drier soils. CLM2 transpiration is lower than in LSM1 because of drier soils, tighter control on transpiration by soil water, and a different canopy conductance scheme. Ground evaporation in CLM2 is lower than in LSM1 because of higher aerodynamic resistance to the transfer of moisture and a thinner surface soil layer. This results in lower latent heat and higher sensible heat, which leads to higher surface temperature and lower precipitation.

2.1.2 Land-cover heterogeneity

In LSM1, vegetation effects are included by specifying one of 28 different biomes for each grid cell. These biomes can consist of multiple plant functional types (PFTs) so that for example, forest crop consists of separate patches of crop, broadleaf deciduous tree, and evergreen needleleaf tree. The type of biome determines the PFT composition of the vegetation and their abundance (Table 1). The PFT determines plant physiology (leaf optical properties, stomatal physiology, leaf dimension) and structure (canopy height, roughness length, displacement height, root profile, leaf and stem area). The use of biomes to set PFT composition and structure homogenizes a heterogeneous land-cover. For example, all needleleaf evergreen forests consist of 75% evergreen needleleaf tree and 25% bare ground; and all needleleaf evergreen trees have a height of 17 m, a maximum leaf area index of 5, and a minimum leaf area of 4.

The advent of high spatial resolution global land-cover and leaf area products derived from satellite data allows for a more accurate depiction of spatial heterogeneity and the ability to separately specify vegetation composition and structure. CLM2 was designed to take advantage of these satellite-derived products (Bonan et al. 2002a). In CLM2, the vegetated portion of a grid

Table 1 Plant functional types and % cover for each biome type in LSM1(Bonan 1996). Only those biomes that are affected by the change in land cover are shown (25–60°N and 130–60°W). NET indicates needleleaf evergreen tree; BDT, broadleaf deciduous tree; WG, warm C_4 grass; CG, cool C_3 grass; C, crop; B, bare ground

Biome	PFT	% Cover	PFT	% Cover	PFT	% Cover
Needleleaf evergreen forest	NET	75	B	25	–	–
Broadleaf deciduous forest	BDT	75	B	25	–	–
Mixed forest	NET	37	BDT	37	B	26
Warm grassland	WG	60	CG	20	B	20
Cool grassland	CG	60	WG	20	B	20
Forest cropland	C	40	BDT	30	NET	30
Cropland	C	85	B	15	–	–

cell is divided into patches of up to 4 of 16 PFTs that differ in physiology and structure. Bare ground is represented as an unvegetated patch occurring among the PFTs. The global distribution of PFTs and their leaf area are determined from satellite data (Bonan et al. 2002b).

For the purposes of this study, LSM1 was reformulated as described in Bonan et al. (2002b) so that it shares the same approach to representing land-cover heterogeneity as CLM2. However, the biogeophysical parametrisations are unchanged from those described in Bonan (1996).

2.2 Modern and natural vegetation datasets

Two paired sets of modern and potential natural PFT distributions at T42 (approximately 2.8° horizontal resolution) were created. The first set replicates the LSM1 biome-derived modern and natural vegetation datasets used by Bonan (1997, 1999). A second set was derived from satellite data. As in Bonan (1997, 1999), differences between modern and natural vegetation for each set were restricted to the continental USA, southern Canada, and northern Mexico (25–60°N and 130–60°W).

In Bonan (1997, 1999), natural vegetation was derived by modifying the LSM1 modern vegetation biomes (Table 1) to correspond with Kuchler's map of natural vegetation. These biome-derived modern and natural vegetation datasets were translated into statistical distributions of coexisting PFT patches in each T42 grid cell so that they could be used in both CLM2 and the restructured version of LSM1.

A second set of satellite-derived modern and natural PFT distributions was created at $0.5° \times 0.5°$ resolution by incorporating the cropland dataset of Ramankutty and Foley (1999). They derived a global representation of permanent croplands for 1992 by calibrating a remotely sensed land-cover classification dataset against cropland inventory data. They also created a dataset of natural vegetation. However, this dataset represents natural vegetation as discrete cover types. Several of these cover types are composed of mixtures of PFTs (e.g., savanna, evergreen/deciduous mixed forest). This is inconsistent with our approach of representing vegetation as continuous fields. Therefore, instead of using the Ramankutty and Foley (1999) natural vegetation dataset directly, we derived natural vegetation by eliminating the crop-covered fraction of the grid cell in the CLM2 satellite-derived modern vegetation data set described in Bonan et al. (2002a). Existing natural vegetation PFTs were expanded to occupy the entire grid cell, with the PFTs retaining their original proportions of fractional cover. Existing natural vegetation was considered to be inadequate to represent a grid cell when it amounted to less than half the grid cell area. In this case, natural vegetation was derived from neighboring grid cells. If one or more of the eight surrounding grid cell neighbors contained at least 50% natural vegetation, then this information was averaged and applied to the grid cell in question; if not, the search was extended an additional 0.5° in every direction from the central grid cell.

The natural vegetation PFT distribution derived by this procedure was acceptable for most of the domain of interest. However, the algorithm performed inadequately in the upper Midwest (40.0° to 49.5°N and 98.0° to 87.0°W) where crops dominate the modern-day landscape and the few non-crop patches rarely represent the expected mix of natural vegetation. In particular, the natural vegetation in much of this region is classified as savanna or grassland (Ramankutty and Foley 1999), yet our algorithm produced forests denser than in regions where forest was expected. Hence, our algorithm was modified by imposing a latitude-dependent tree-cover limit, starting with 50% maximum tree cover at about 40°N and ending with 85% maximum tree cover at 49°N. This limit was then modified using dominant vegetation information from the natural vegetation data set of Ramankutty and Foley (1999), so that savanna and grassland grid cells would have less tree cover than forests (starting at 40% and 30% maximum tree cover, respectively, instead of 50% at 40°N).

PFT distributions for modern vegetation were derived by incorporating the cropland fractions from Ramankutty and Foley (1999) for the year 1992 and reducing the patches of natural vegetation proportionally. This methodology resulted in a slightly different modern vegetation dataset than the one normally used by CLM2. However, the new modern dataset is fully consistent with Ramankutty and Foley's (1999) historical croplands datasets for 1700–1992 and thus enables future research exploring climate sensitivity to land-cover change at other slices in time. It is also expected to be more accurate with respect to cropland fraction because of the link to agricultural inventory data and the fact that subpixel variations in cropland fraction were accounted for.

Leaf area for the biome-derived modern and natural vegetation datasets is from LSM1 (Bonan 1996). Values are updated daily using prescribed monthly values from Dorman and Sellers (1989) for each PFT. Leaf area for the satellite-derived modern and natural vegetation datasets used present-day satellite data. For grid cells where a PFT was added that did not occur in the present-day satellite data (e.g., cropland versus forest), there was no valid leaf area and instead an average leaf area was obtained for that PFT from surrounding grid cells.

2.3 Experimental design

Bonan (1997) and Bonan (1999) used the NCAR LSM1 coupled to the NCAR Community Climate Model version 2 (CCM2) and version 3 (CCM3), respectively. Here, simulations of 20-year length were performed with

each of the two land models coupled to the Community Atmosphere Model (CAM version 2) (Collins et al. 2003). CAM2 is the successor to the NCAR CCM3 and features improvements in atmospheric simulation related to the addition of a prognostic cloud-water parametrisation and a new radiation package. CAM2 is configured at T42 resolution with 26 levels in the vertical and a 20-min time step. Simulations used climatological sea surface temperatures. The land models were initialized with temperatures of 10 °C, no snow or canopy water, and volumetric soil water content of 0.3 mm^3/mm^{-3} over land. Lakes and wetlands were initialized to 4 °C. Glaciers were initialized to –23 °C and 1000 kg/m^{-2} of snow. The last 15 years of the simulations were analyzed to allow a 5-year spinup of soil water and temperature.

Eight simulations, four paired modern and natural vegetation simulations, were conducted to address whether the conclusions of Bonan (1997,1999) are robust in the context of different land surface and atmospheric models and improved land-cover change datasets (Table 2). The BIOME_LSM experiment is first compared to the results of Bonan (1997, 1999) and addresses the impact of a different atmospheric model (Sect. 3.2). The SAT_LSM experiment is compared with BIOME_LSM to examine the impact of improved land-cover change datasets in the context of LSM1 as the land model (Sect. 3.3). The BIOME_CLM experiment is compared to BIOME_LSM to examine the impact of a different land-surface model in the context of biome-derived land-cover change (Sect. 3.4). Finally, we compare SAT_CLM with BIOME_LSM to evaluate the impact of a combination of a different land-surface model and improved land-cover change datasets (Sect. 3.5).

The land-cover change forcing in these experiments is derived from the changes in natural PFT distribution associated with the introduction of the crop PFT and the differences in PFT morphological, optical, and photosynthetic properties (Bonan 1996, 1998; Bonan et al. 2002a). In addition, crops are given loam soil texture to better reflect the properties of organic soils associated with agriculture as in Bonan (1997, 1999). An important property of the PFTs differs between LSM1 and CLM2. The maximum carboxylation rate used in the photosynthesis-stomatal conductance model is higher in LSM1 for crops (50 $\mu mol/m^2/s$) than other PFTs (33 $\mu mol/m^2/s$). Due to changes in the canopy conductance scheme, this difference is eliminated in CLM2.

Table 2 Description of land cover change experiments. Each experiment consists of a modern vegetation simulation and a natural vegetation simulation

Experiment	Land-cover change dataset	Model
BIOME_LSM	Biome-derived	LSM1
SAT_LSM	Satellite-derived	LSM1
BIOME_CLM	Biome-derived	CLM2
SAT_CLM	Satellite-derived	CLM2

3 Results

3.1 Modern and natural vegetation datasets

The spatial distribution of differences between modern and natural vegetation for the primary PFTs in the biome-derived and satellite-derived experiments is shown in Figs. 1 and 2, respectively, and summarized by region in Table 3. Both datasets show intense agricultural activity east of 100°W that has replaced the natural vegetation consisting of mixtures of grass, and broadleaf deciduous and needleleaf evergreen trees. However, there are several notable differences between the two representations of land-cover change that have implications for the response of the climate system. Cropland-cover in the biome-derived dataset is generally overestimated compared to the satellite-derived dataset east of 100°W, particularly in the Northeast region (Table 3). In contrast, the satellite-derived dataset indicates that agricultural development extends a bit further west than the biome-derived dataset and picks up additional scattered regions of development in the western USA and southwestern Canada. These differences alone imply that the land-cover change forcing due to the introduction of crops may be somewhat diminished east of 100°W and slightly stronger west of 100°W in the satellite-derived dataset compared to the biome-derived dataset.

The land-cover change forcing is also affected because of differences in the types of natural vegetation cover that are replaced by cropland. Bonan (1999) noted in his experiments that the biome-derived natural forest cover west of the Mississippi River and in parts of the Midwest was likely overestimated at the expense of grasslands. Indeed, the natural vegetation distribution derived from satellite data indicates more extensive grasslands east of 100°W. In the North Central and South regions, nearly 50% of the natural vegetation is grassland (Table 3). Since the ecological properties associated with crops are more similar to grasses than to trees, the land-cover change forcing due to ecological differences between PFTs is reduced in the satellite-derived dataset.

The bare ground fraction in the biome-derived datasets is significantly reduced due to crops but unchanged in the satellite-derived datasets. The reduction in bare ground in the biome-derived datasets is due to the prescribed bare-ground fraction associated with each biome (Table 1). The satellite-derived datasets have no bare ground. This is because the algorithm used to derive leaf area from satellite data assumes that the leaf area is distributed uniformly within a given PFT patch. A bare-soil patch is specified only when the satellite-derived leaf area is zero. This has important implications for assessing the impact of model biogeophysics as discussed in Sect. 3.4.

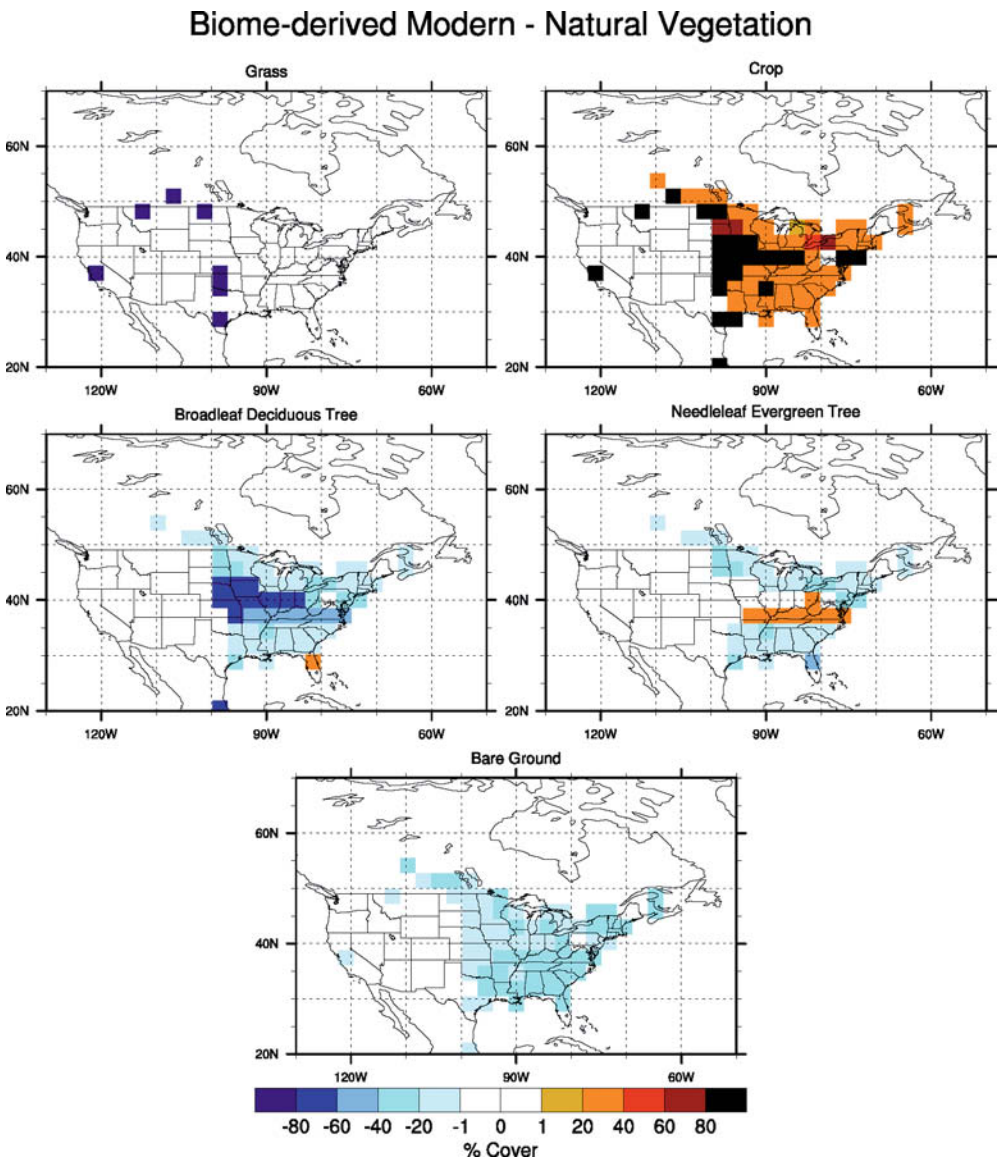

Fig. 1 Differences in percent cover of plant functional types between biome-derived modern and natural vegetation datasets

3.2 Impact of atmospheric model

Bonan (1997) concluded that modern vegetation causes cooling in spring over the eastern USA and in summer over the central USA. Bonan (1999) found cooling in summer and autumn daily mean temperature in eastern and central USA as well as a reduction in the diurnal temperature range. In this section, we compare the results of the BIOME_LSM experiment with the results of Bonan (1997, 1999) to assess the impact of using a different atmospheric model.

The replacement of natural vegetation by modern vegetation using the biome-derived datasets and LSM1 resulted in cooling over nearly all of the USA in summer and autumn (Fig. 3a). The cooling is statistically significant at the 90% confidence level over the Northeast, North Central, and South regions and was generally stronger in summer than autumn (Fig. 4). The maximum cooling in summer and autumn was >2.0 °C and >1.0 °C, respectively, and was centered on the region with the most intensive agriculture (Fig. 1). Changes in winter and spring were smaller and not statistically significant.

The cooling was stronger for daily maximum than daily minimum temperature resulting in a reduced diurnal temperature range, particularly in the North Central region of the USA (Table 4). In summer and autumn, the daily maximum temperature was reduced by 0.9–2.4 °C while the diurnal temperature range was reduced by 0.4–1.8 °C. Only the reduction in autumn diurnal temperature range in the South region was not significant at the 95% confidence level.

Bonan (1997, 1999) described the changes in ecological parameters that caused summer and autumn cooling. As a result of natural vegetation being replaced by croplands, summer and autumn albedo increased, roughness length decreased, the sum of leaf and stem area decreased, and stomatal resistance decreased. In the

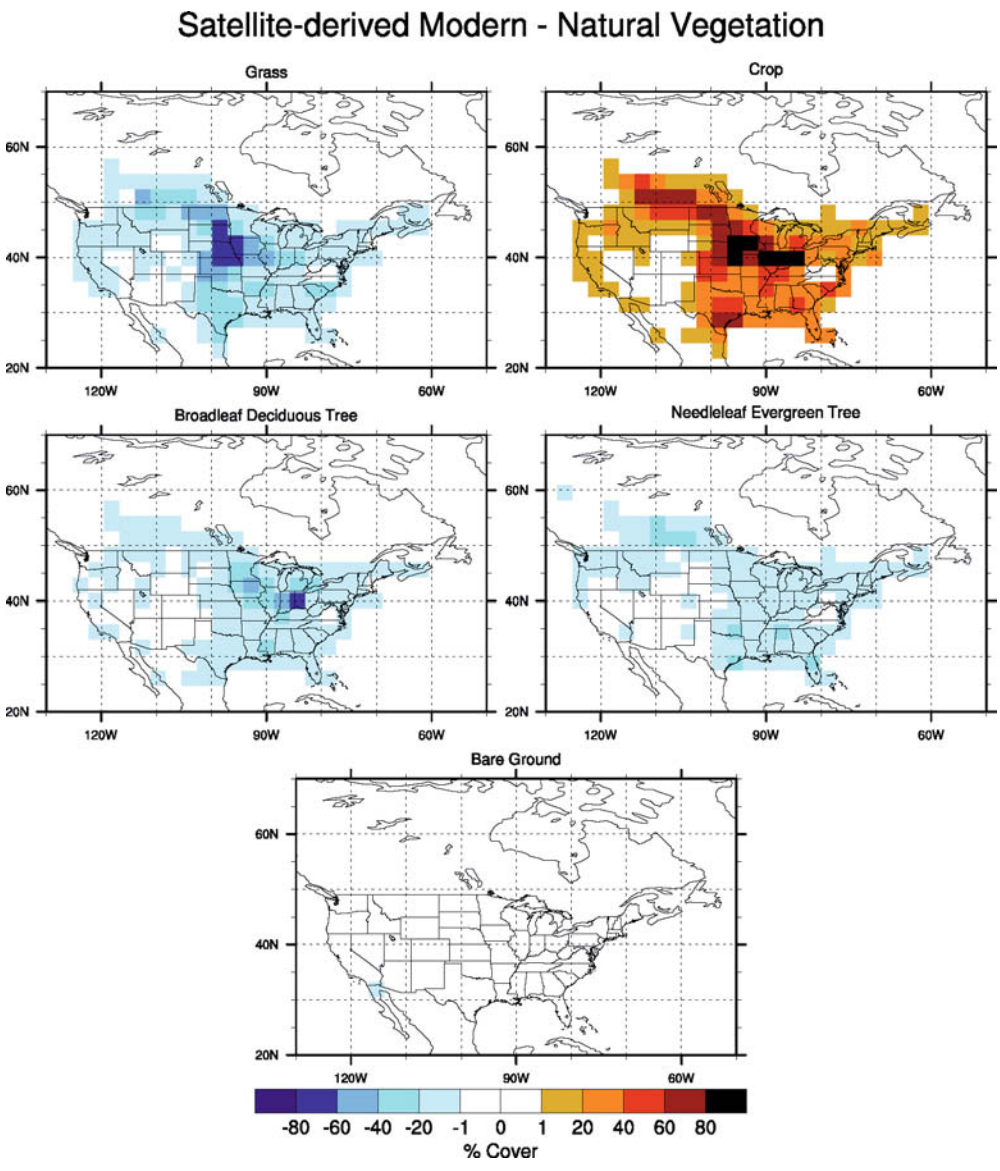

Fig. 2 As in Fig. 1 but for the satellite-derived modern and natural vegetation datasets

North Central region of the USA for example, the summer albedo increased which reduced the solar radiation absorbed by the vegetation (Table 5). The reduced absorbed solar radiation was offset somewhat by decreased longwave loss to the atmosphere so that net radiation (absorbed solar– net longwave) decreased by

Table 3 Summary of land cover change in the biome-derived and satellite-derived experiments for three geographic regions of the USA

Plant functional type	Northeast		North Central		South	
	Biome-derived	Satellite-derived	Biome-derived	Satellite-derived	Biome-derived	Satellite-derived
Crop	30 (0)	16 (0)	57 (0)	54 (0)	43 (0)	36 (0)
Grass	0 (0)	22 (27)	0 (3)	19 (50)	0 (5)	32 (49)
Broadleaf deciduous tree	18 (34)	27 (35)	10 (49)	10 (26)	24 (32)	11 (20)
Needleleaf evergreen tree	32 (33)	25 (28)	13 (14)	6 (13)	24 (32)	20 (30)
Bare ground	10 (23)	0 (0)	9 (23)	0 (0)	3 (25)	0 (0)
Shrub	0 (0)	0 (0)	0 (0)	0 (0)	5 (5)	0 (0)

Values are the percent cover in each region for modern vegetation with values for natural vegetation in parentheses. The remainder of the region that is not covered by the listed plant functional types is lake and/or wetland, which do not differ between modern and natural vegetation datasets and between biome-derived and satellite-derived experiments. Regions are defined for land points only as follows: Northeast (37–50°N, 85–60°W), North Central (37–50°N, 100–85°W), South (30–37°N, 100–60°W)

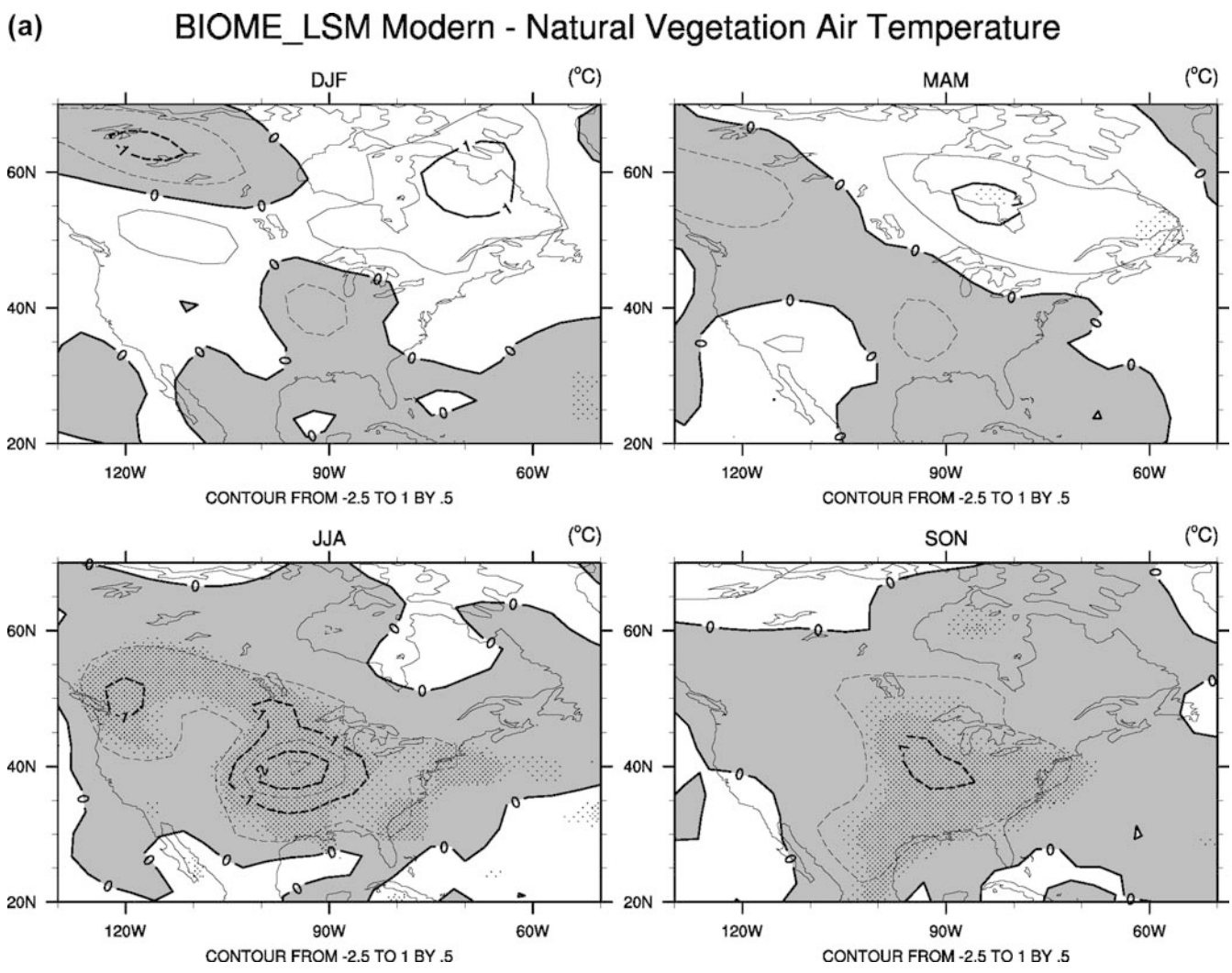

Fig. 3 Effects of modern vegetation on winter (DJF), spring (MAM), summer (JJA), and autumn (SON) air temperature for the **a** BIOME_LSM experiment which uses biome-derived modern and potential vegetation datasets and LSM1 as the land model as described in the text, **b** SAT_LSM experiment which uses the satellite-derived modern and potential vegetation datasets and LSM1 as the land model, and **c** the SAT_CLM experiment which uses the satellite-derived modern and potential vegetation datasets and CLM2 as the land model. *Shading* indicates cooling (modern – natural vegetation). *Light* and *dense stippling* indicates regions where the difference is statistically significant ($P < 0.1$ and $P < 0.05$, respectively)

7 W/m^2. This was balanced by a 19 W/m^2 decrease in sensible heat flux and a 12 W/m^2 increase in latent heat flux. Total sensible and latent heat fluxes are a sum of the individual contributions from vegetation and soil. The reduction in sensible heat flux was caused by reduced vegetation sensible heat offset somewhat by increased ground sensible heat due in part to increased solar radiation forcing. The increase in latent heat was caused by increases in canopy evaporation, transpiration, and ground evaporation.

Atmospheric forcing of the land-surface also appeared to play a role in the summer cooling. There was a statistically significant increase in precipitation in the North Central region (Table 5). This contributed to increased canopy evaporation and wetter soils (as implied by the increase in the btran parameter). Wetter soils and decreased stomatal resistance increased transpiration and ground evaporation and reduced sensible heat. In addition, the incoming radiation (solar plus longwave) decreased by 8 W/m^2 which reduced the heat loading on vegetation and soil.

The autumn cooling, although smaller than in summer, appeared to be due to similar mechanisms; reductions in absorbed solar radiation, net radiation, and sensible heat (Table 6). However, latent heat was essentially unchanged because an increase in transpiration was offset by decreases in canopy and ground evaporation. Thus, a decrease in net radiation (4 W/m^2) was nearly balanced by a similar decrease in sensible heat alone. Atmospheric forcings favorable to cooling were also not as prominent as in summer. There was no change in precipitation and the incoming radiation decreased by 4 W/m^2 compared to a decrease of 8 W/m^2 in summer.

These results are similar to Bonan (1997, 1999) except that Bonan (1999) showed stronger cooling in autumn than summer while Bonan (1997) showed cooling in

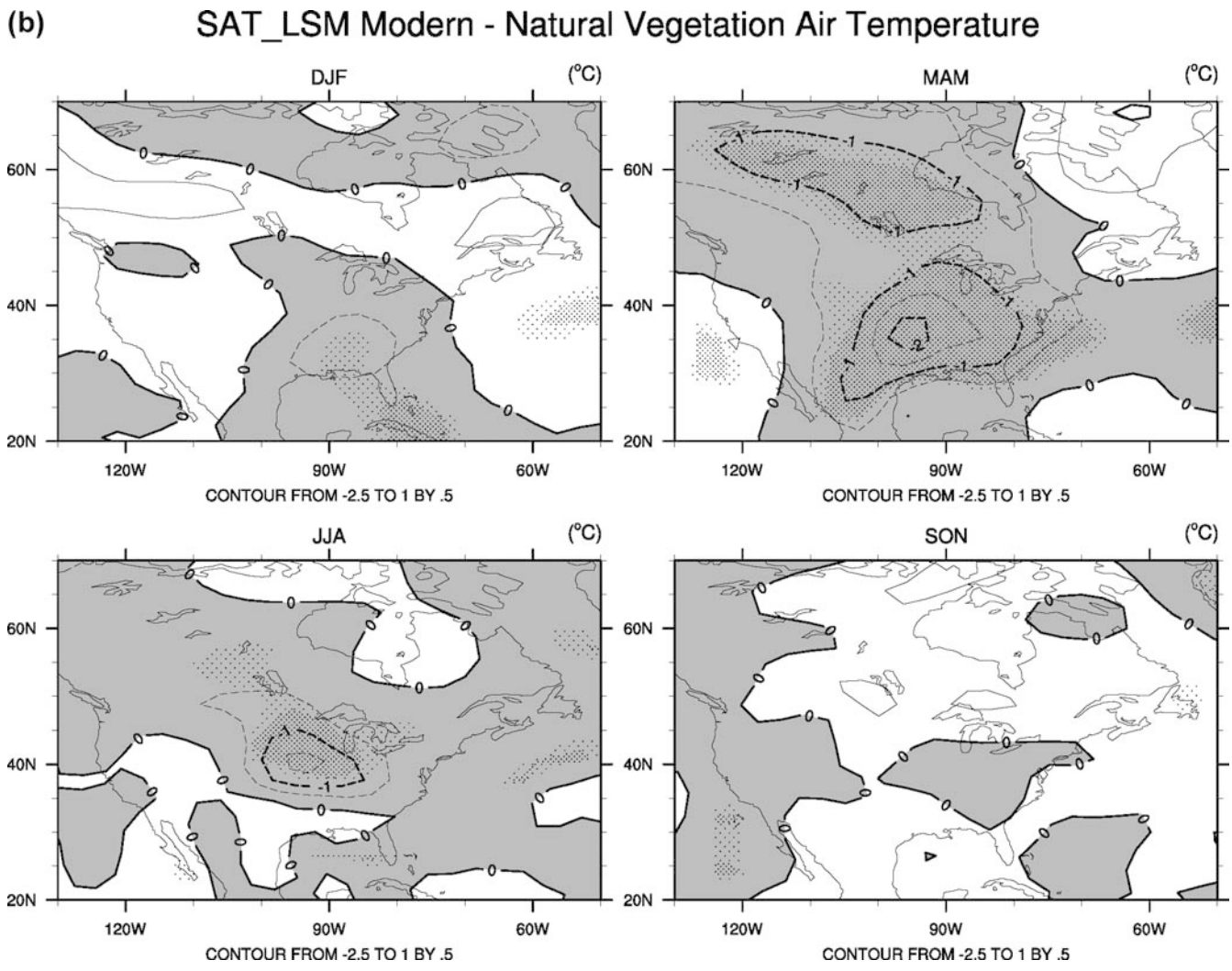

Fig. 3 (Contd.)

spring and summer and did not detect autumn cooling. Factors causing this disparity could include effects from the atmospheric model, SST boundary conditions, and the length of the simulations. However, the conclusions of Bonan (1997, 1999) that the North American human-impacted landscape cools summer climate and reduces the diurnal temperature range, appears to be robust when a different atmospheric model is used.

3.3 Impact of satellite-derived land-cover change datasets

In this section, we examine the impact of using improved satellite-derived land-cover change datasets to describe the land-cover change forcing (SAT_LSM). In the context of LSM1 as the land-surface model, the use of satellite-derived datasets diminishes both the magnitude and spatial extent of cooling in summer and autumn and enhances spring cooling compared to the use of biome-derived datasets (BIOME_LSM) (Fig. 3b). The diminished cooling in summer differs significantly at the 90% confidence level from BIOME_LSM only in the southern USA while autumn is significantly warmer than BIOME_LSM in all regions (Fig. 4). The enhanced spring cooling is significantly different in all regions as well. The reduction in diurnal temperature range is somewhat smaller compared to BIOME_LSM but is still significant for all regions (Table 4).

In summer, the strongest cooling was >1.5 °C and remained centered on the North Central USA, the region with the most intensive agricultural activity (Fig. 3b). The diminished cooling can likely be explained by a combination of the two factors discussed in Sect. 3.1. First, the land-cover change in SAT_LSM is from a grass/tree mixture to crops while the change in BIOME_LSM is primarily forest to croplands (Figs. 1, 2, Table 3). The ecological properties associated with crops are more similar to grasses than to trees. For example, the increase in albedo in the North Central region is much smaller in SAT_LSM because prescribed optical properties of crops and grasses are identical (Table 5).

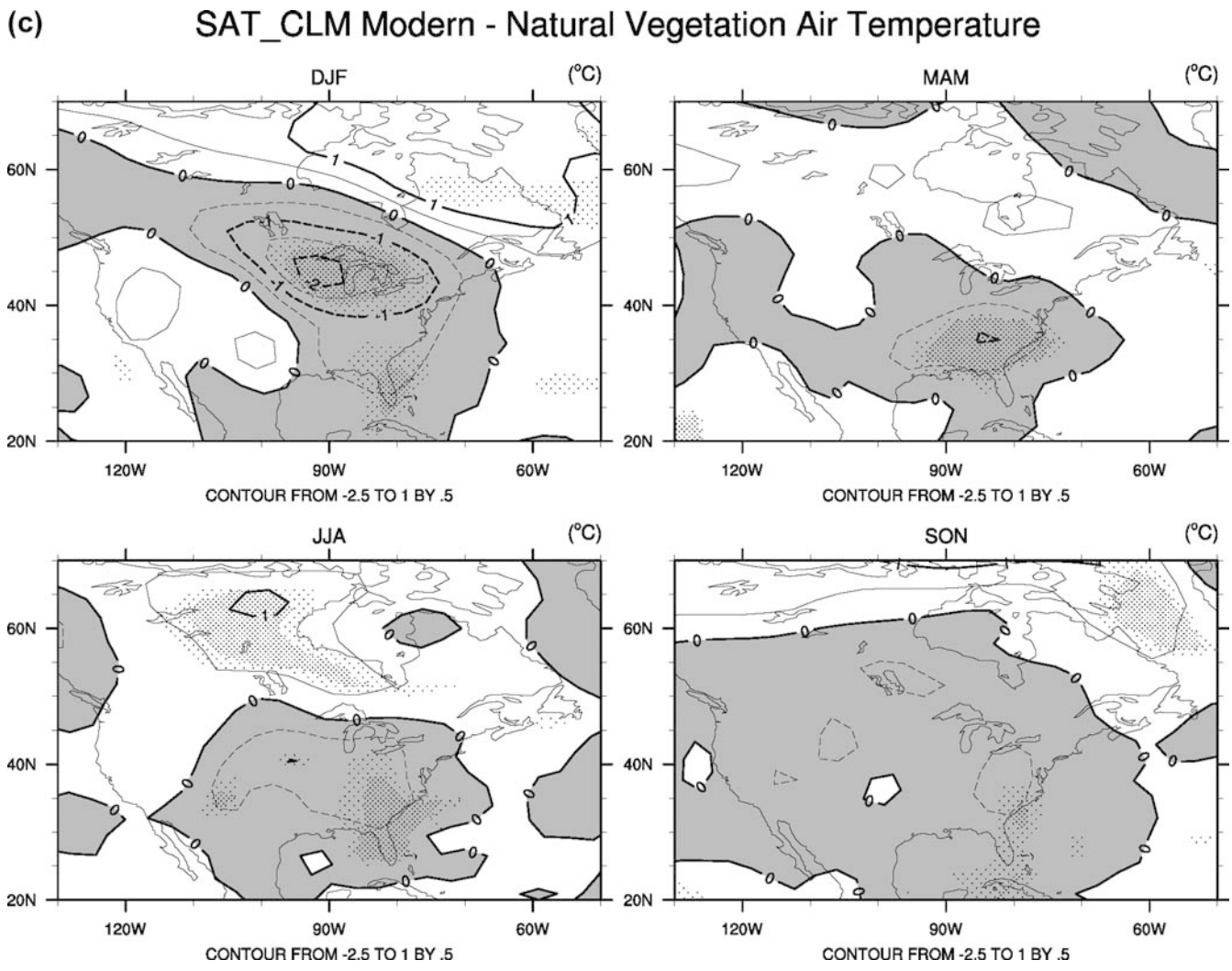

Fig. 3 (Contd.)

Secondly, the intensity of agriculture in the satellite-derived modern dataset is somewhat less than in the biome-derived dataset (Table 3). As a result of these factors, the decreases in absorbed solar radiation, net radiation, and sensible heat and increase in latent heat were not as pronounced in the SAT_LSM experiment (e.g., Table 5).

In the southern USA the replacement of natural vegetation by satellite-derived modern vegetation has no discernible effect on summer temperature (Table 7). This differs significantly from the BIOME_LSM experiment. The SAT_LSM summer albedo forcing is comparable to BIOME_LSM (an increase of 1% absolute), resulting in lower net radiation. However, in SAT_LSM the decrease in net radiation is mostly balanced by a decrease in sensible heat with little change in latent heat while there is a substantial increase in latent heat, primarily due to transpiration, in BIOME_LSM. The land-cover change forcing in terms of leaf area is also quite different between the two experiments. The BIOME_LSM experiment has an increase in leaf area that may contribute to the increase in transpiration while SAT_LSM has a decrease. Unfavorable changes in atmospheric forcing compared to BIOME_LSM also may contribute. Precipitation decreased by 0.1 mm/day and incoming radiation increased by 2 W/m^2 as compared to an increase in precipitation of 0.1 mm/day and a decrease in incoming radiation of 3 W/m^2 in BIOME_LSM (Table 7).

There were essentially no changes in autumn temperature in the SAT_LSM experiment in all regions (Fig. 4). This differs significantly from the BIOME_LSM experiment in which cooling was found. This is likely due to a large reduction in the albedo forcing. In the North Central region, for example, the albedo forcing in SAT_LSM is nearly zero (Table 6) due to the identical optical properties of grasses and crops. There were still significant reductions in diurnal temperature range of 0.4–1.0 °C in autumn (Table 4). In contrast to summer however, the reduction was due to nearly equal decreases in the daily maximum temperature and increases in daily minimum temperature such that the daily mean temperature was nearly unchanged.

Table 4 Differences (modern minus natural vegetation) in summer (June, July, August) and autumn (September, October, November) daily minimum temperature, daily maximum temperature, and diurnal temperature range for three geographic regions of the United States

	Northeast			North Central			South		
Season	Low	High	Range	Low	High	Range	Low	High	Range
	BIOME_LSM								
Summer	–0.1	–0.9**	–0.8**	–0.6**	–2.4**	–1.8**	–0.5**	–1.2**	–0.7**
Autumn	–0.2	–0.9**	–0.7**	–0.4	–1.4**	–1.0**	–0.5**	–0.9**	–0.4
	SAT_LSM								
Summer	–0.1	–0.5**	–0.4**	–0.4	–1.7**	–1.3**	0.1	–0.3	–0.4*
Autumn	0.3	–0.1	–0.4**	0.4	–0.4	–0.8**	0.5	–0.5	–1.0**
	BIOME_CLM								
Summer	–0.3	–0.7*	–0.4**	0.1	–0.9*	–1.0**	0.1	0	–0.1
Autumn	0.1	–0.2	–0.3**	0.4	–0.2	–0.6**	0.3	0	–0.3
	SAT_CLM								
Summer	0.1	–0.4	–0.5**	–0.2	–0.8*	–0.6**	–0.1	–1.1**	–1.0**
Autumn	–0.3	–0.5	–0.2*	0	–0.7	–0.7**	–0.1	–0.6*	–0.5**

Temperatures (°C) are from an average diurnal cycle at 1-h resolution. *$P < 0.10$, **$P < 0.05$. Regions are defined for land points only as follows: Northeast (37–50°N,85–60°W), North Central (37–50°N, 100–85°W), South (30–37°N, 100–60°W). The experiments are described in Table 2

The enhanced spring cooling in SAT_LSM appears to be due to a combination of higher albedo, increased latent heat and decreased sensible heat, and somewhat more favorable atmospheric forcing (increased precipitation, reduced incoming radiation) compared to BIOME_LSM. In the South region, for example, the albedo forcing in the SAT_LSM experiment was twice that of BIOME_LSM (Table 8). The albedo forcing was larger despite the fact that a significant part of the natural vegetation that is replaced by crops is grass (Table 3). However, in BIOME_LSM, 25% of the natural vegetation in the South region consists of bare soil and is replaced by vegetation, which generally has lower albedo than bare soil. This offsets some of the increase in albedo where crops replace trees.

Increased spring latent heat flux in SAT_LSM compared to BIOME_LSM was caused by higher transpiration. Transpiration decreased in BIOME_LSM and increased in SAT_LSM even though the water availability, as indicated by the "Btran" parameter, increased in both cases. In BIOME_LSM, the prescribed leaf area for crops is zero until May. Thus, there is no transpiration for crop patches in March and April. The SAT_LSM leaf area for crops in these months is nonzero and hence transpiration can occur and be affected by increases in water availability.

Table 5 Differences (modern minus natural vegetation) in summer surface climatology using LSM1 as the land model with biome-derived (BIOME_LSM) and satellite-derived (SAT_LSM) datasets, and CLM2 as the land model with biome-derived (BIOME_CLM) and satellite-derived (SAT_CLM) datasets for the North Central (37–50°N, 100–85°W) region of the USA

Variable	BIOME_LSM	SAT_LSM	BIOME_CLM	SAT_CLM
Air temperature (°C)	–1.5**	–1.0**	–0.4	–0.5
Precipitation (mm/day)	0.4**	0.2	–0.1	0.0
Albedo (%)	2.2**	0.7**	2.2**	0.8**
Incoming solar radiation (W/m^2)	–7.4**	–10.4**	1.1	0.8
Absorbed solar radiation (W/m^2)	–12.7**	–10.6**	–5.7**	–1.5
Vegetation	–18.7**	–16.9**	–14.4**	–10.2**
Ground	6.0**	6.3**	8.7**	8.7**
Incoming longwave (W/m^2)	–0.6	0.5	–0.3	–0.3
Net longwave (W/m^2)	–6.1**	–5.3**	3.5	–0.3
Sensible heat (W/m^2)	–18.5**	–10.3**	–8.0**	–4.7**
Vegetation	–23.5**	–16.9**	–7.3**	–6.9**
Ground	5.1**	6.6**	–0.7*	2.1**
Latent heat (W/m^2)	12.0**	4.9	–1.6	4.3
Canopy evaporation	2.1**	0.7	–2.0*	–0.5
Transpiration	6.5**	7.6**	2.6*	3.5**
Ground evaporation	3.4*	–3.5**	–2.1**	1.3**
Btran (–)	0.2**	0.1**	0.1	0.0
Leaf area index (m^2/m^2)	–0.3**	0.0**	–0.3**	0.0**
Stem area index (m^2/m^2)	–0.4**	–0.5**	–0.4**	–0.5**

Net longwave is defined as positive from land to atmosphere. Btran is a parameter describing the limiting effect of soil moisture on transpiration and ranges from 0 (soil water limits transpiration completely) to 1 (transpiration not limited by soil water).
*$P < 0.10$, **$P < 0.05$

Table 6 As in Table 5 but for autumn

Variable	BIOME_LSM	SAT_LSM	BIOME_CLM	SAT_CLM
Air temperature (°C)	–0.9**	0.1	0.1	–0.3
Precipitation (mm/day)	0.0	0.1	–0.2	0.0
Albedo (%)	2.4**	0.1	2.8**	0.3**
Incoming solar radiation (W/m^2)	–3.9**	–3.5	3.0*	0.0
Absorbed solar radiation (W/m^2)	–6.9**	–2.9	–1.8	–0.4
Vegetation	–27.9**	–17.1**	–25.8**	–15.0**
Ground	21.0**	14.3**	24.0**	14.6**
Incoming longwave (W/m^2)	–0.1	2.8	0.4	0.8
Net longwave (W/m^2)	–3.1	–2.1	4.2**	1.4
Sensible heat (W/m^2)	–3.9**	–5.6**	–3.1**	–2.2*
Vegetation	–11.2**	–7.4**	–7.0**	–3.6**
Ground	7.3**	1.8**	3.9**	1.4**
Latent heat (W/m^2)	0.5	4.3**	–2.1	0.2
Canopy evaporation	–0.8**	–0.2	–2.4**	–1.9**
Transpiration	1.6**	2.5**	0.6**	1.0**
Ground evaporation	–0.3	1.9*	–0.3	1.1*
Btran (–)	0.1**	0.1**	–0.1**	0.0
Leaf area index (m^2/m^2)	0.0**	–0.2**	0.0**	–0.2**
Stem area index (m^2/m^2)	–0.6**	–0.5**	–0.6**	–0.5**

In summary, we conclude that the summer cooling and reduction in diurnal temperature range associated with human-induced land-cover change is robust in the context of improved land-cover datasets. In addition, we find that this more realistic depiction of land-cover change causes a statistically significant cooling in the spring over much of the USA.

3.4 Impact of model biogeophysics

In this section, we examine the impact of using a different land-surface model in the context of biome-derived land-cover forcing (BIOME_CLM). There are no statistically significant changes in surface temperature (at the 90% confidence level) in the BIOME_CLM experiment in any season for any region (Fig. 4). This differs significantly from BIOME_LSM for the North Central and South regions in summer and for all regions in autumn. The BIOME_CLM experiment shows cooling in the North Central region in summer, however, the cooling is reduced by about 1 °C from BIOME_LSM and is not statistically significant (Table 5). In the Northeast region, the cooling in BIOME_CLM is comparable to BIOME_LSM. In both cases, interannual variability in BIOME_CLM appears to be larger than in BIOME_LSM, which makes a statistically significant signal more difficult to detect. However, there are significant reductions in the summer and autumn diurnal temperature range in the Northeast and North Central regions, although the reduction is about half that of BIOME_LSM (Table 4). The largest reduction occurred in summer in the region with the largest land-cover change.

In the North Central region in summer, an increase in albedo in BIOME_CLM resulted in lower absorbed solar radiation by the vegetation-soil system, as in BIOME_LSM (Table 5). Sensible heat decreased in both experiments, however, latent heat decreased in BIOME_CLM and increased in BIOME_LSM. Canopy evaporation and ground evaporation both decreased while transpiration experienced only a small increase compared to BIOME_LSM. The atmospheric forcing changes favorable to cooling in the BIOME_LSM experiment were lacking in BIOME_CLM. There was an increase of about 1 W/m^2 in incoming radiation compared to a decrease of 8 W/m^2 in BIOME_LSM. Similarly, precipitation decreased by 0.1 mm/day compared to an increase of 0.4 mm/day in BIOME_LSM. Similar behavior in summer sensible and latent heat and atmospheric forcing can be seen in the South region (Table 7).

Atmospheric forcing may also play a role in eliminating the autumn cooling seen in BIOME_LSM. BIOME_CLM had decreases in precipitation of 0.2 mm/day, 0.2 mm/day, and 0.3 mm/day and increases in incoming radiation of 2 W/m^2, 3.5 W/m^2, and 4 W/m^2 for the Northeast, North Central, and South regions, respectively (e.g., Table 6). The BIOME_LSM experiment generally had slightly increased or unchanged precipitation and decreased incoming radiation. These atmospheric forcing differences likely contributed to increased absorbed solar radiation, drier soils, lower latent heat, and higher sensible heat in BIOME_CLM compared to BIOME_LSM, which resulted in warmer temperatures.

The summer and autumn land-cover change forcing in BIOME_CLM in terms of albedo and leaf and stem area is generally similar to that in BIOME_LSM (e.g., Tables 5, 6, 7). Changes in roughness are also the same since the two experiments share identical changes in PFT distribution, and roughness lengths and displacement heights do not differ between models. However, the decrease in unstressed minimum stomatal resistance that occurs when trees are replaced by crops in LSM1 (Bonan 1997, 1999) is not likely to be as large in CLM2 because of similarity in photosynthetic parameters of crops and trees.

The response of CLM2 to changes in solar radiation absorbed by the soil may also play a role. In the North

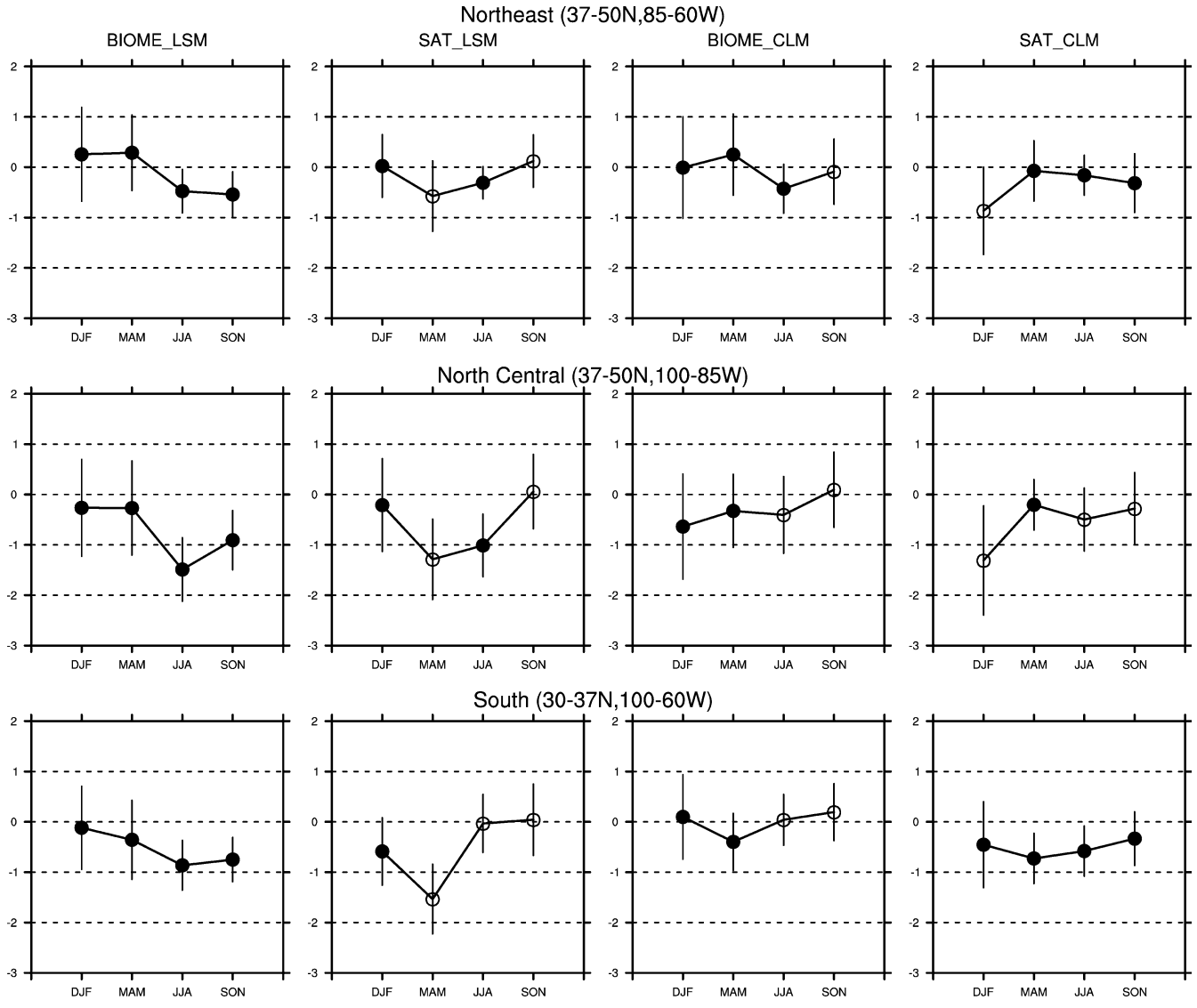

Fig. 4 Differences (modern – natural vegetation) in the mean seasonal air temperature for three geographic regions of the USA. The four experiments are LSM1 as the land model with biome-derived (BIOME_LSM) and satellite-derived (SAT_LSM) datasets, and CLM2 as the land model with biome-derived (BIOME_CLM) and satellite-derived (SAT_CLM) datasets. *Open circles* represent a mean temperature that is significantly different from the BIOME_LSM experiment. The *error bars* represent the 90% confidence interval computed from the Student *t*-statistic

Central region for example, solar radiation absorbed by the ground increased due to decreased canopy density (Fig. 5). LSM1 responded with increased sensible and latent heat so that the ground temperature was unchanged. In contrast, CLM2 responded with decreased ground sensible and latent heat and the ground warmed by 3.6 °C. This greatly increased the longwave radiation from ground to canopy and warmed the canopy and air. The reduction in ground turbulent fluxes in CLM2 is related to the elimination of bare ground in the biome-derived modern vegetation dataset. CLM2 has much higher aerodynamic resistance to heat and moisture transfer for soil beneath canopy compared to soil with no canopy (bare ground) (Bonan et al. 2002a). The corresponding resistances in LSM1 are more similar. Thus, a reduction in bare ground in CLM2 means that more of the soil is beneath the canopy and is therefore subject to the higher aerodynamic resistance. Furthermore, the aerodynamic resistance for soil beneath canopy in CLM2 is substantially higher than the corresponding resistance in LSM1 (Bonan et al. 2002a), making CLM2 ground temperature more sensitive to increases in solar forcing. Further evidence for this conclusion is that the SAT_CLM experiment, which involves no changes in bare ground, has the same increase in ground-absorbed solar radiation (about 9 W/m^2, Table 5), but responds with an increase in the turbulent fluxes of 3.4 W/m^2 and an increase in ground temperature of less than 1 °C.

The strongest summer cooling in BIOME_LSM appears to be associated with a positive atmospheric feedback in which an increase in latent heat leads to

Table 7 As in Table 5 but for the summer surface climatology for the South region of the USA (30–37°N, 100–60°W)

Variable	BIOME_LSM	SAT_LSM	BIOME_CLM	SAT_CLM
Air temperature (°C)	–0.9**	0.0	0.0	–0.6*
Precipitation (mm/day)	0.1	–0.1	–0.1	0.2
Albedo (%)	0.9**	0.9**	0.6**	1.0**
Incoming solar radiation (W/m^2)	–2.6	2.6	2.2	–3.4
Absorbed solar radiation (W/m^2)	–5.1**	–0.6	0.0	–6.0**
Vegetation	17.4**	–19.1**	20.7**	–23.2**
Ground	–22.4**	18.5**	–20.7**	17.2**
Incoming longwave (W/m^2)	–0.4	–0.2	–0.8	1.8*
Net longwave (W/m^2)	–2.4	3.0	3.4	–1.0
Sensible heat (W/m^2)	–12.3**	–4.6	–3.0	–9.9**
Vegetation	–4.1*	–15.5**	8.5**	–12.8**
Ground	–8.2**	10.9**	–11.4**	2.9**
Latent heat (W/m^2)	9.2**	0.2	–0.6	5.1
Canopy evaporation	2.8**	–1.1	3.6*	1.0
Transpiration	11.4**	2.2	3.6**	1.0
Ground evaporation	–5.0**	–0.9	–7.9**	2.4**
Btran (–)	0.1**	0.0	0.1**	0.0
Leaf area index (m^2/m^2)	0.3**	–0.5**	0.3**	–0.5**
Stem area index (m^2/m^2)	–0.2**	–0.3**	–0.2**	–0.3**

increased precipitation and wetter soils. The increase in precipitation may be due to local recycling of the water from an increase in transpiration that results when crops replace trees. This feedback is absent in BIOME_CLM, possibly because of the fact that crops do not transpire more than trees in CLM2. Additionally, several of the parametrisations that make CLM2 a warmer, drier model are related to transpiration (Bonan et al. 2002a). CLM2 has tighter control on transpiration by soil water and a different canopy conductance scheme in which only sunlit leaves photosynthesize and transpire.

We conducted an additional experiment (BIOME_CLM_TR) to test the hypothesis that these parametrisations are primarily responsible for the differences in the response of CLM2 and LSM1 to land-cover change. We replaced CLM2 parametrisations related to transpiration with those from LSM1. The maximum rate of carboxylation for crops was increased by an amount proportional to the increase prescribed in LSM1. LSM1 parametrisations for soil water control of stomatal resistance and canopy integration replaced those in CLM2. We also implemented a new parametrisation for the aerodynamic resistance to heat and moisture transfer for soil beneath canopy that is proposed for the next model version. The new parametrisation eliminates unrealistic sensitivity of soil temperature in CLM2 to changes in leaf and stem area.

Implementation of the new parametrisations in CLM2 resulted in stronger summer cooling in the North Central region compared to BIOME_CLM (Table 9). The cooling of 1.2 °C is statistically significant at the 95% level and is comparable to the 1.5 °C cooling in BIOME_LSM. As anticipated, the modified CLM2 produced higher latent heat, lower sensible heat, more precipitation, and wetter soils compared to BIOME_CLM, which resulted in cooler temperatures. The

Table 8 As in Table 5 but for the spring surface climatology for the South region of the USA (30–37°N, 100–60°W)

Variable	BIOME_LSM	SAT_LSM	BIOME_CLM	SAT_CLM
Air temperature (°C)	–0.4	–1.5**	–0.4	–0.7**
Precipitation (mm/day)	0.3	0.4**	0.0	0.3**
Albedo (%)	0.6**	1.2**	0.8**	1.2**
Incoming solar radiation (W/m^2)	–6.7	–8.0**	0.7	–4.6*
Absorbed solar radiation (W/m^2)	–7.3**	–9.8**	–1.5	–7.2**
Vegetation	–23.5**	–24.6**	–20.3**	–22.8**
Ground	16.3**	14.8**	18.8**	15.6**
Incoming longwave (W/m^2)	1.7	–2.1	0.1	0.9
Net longwave (W/m^2)	–1.9	–5.7**	3.4	–2.2
Sensible heat (W/m^2)	–9.1*	–14.2**	–5.2*	–11.1**
Vegetation	–12.8**	–19.7**	–6.5**	–13.5**
Ground	3.7	5.5*	1.3	2.5**
Latent heat (W/m^2)	4.3	10.4**	–0.9	5.8**
Canopy evaporation	0.6	0.7	–2.2**	–0.8
Transpiration	–1.2	4.5**	–0.9	2.5**
Ground evaporation	4.9	5.2**	2.2	4.1**
Btran (–)	0.2**	0.2**	0.0	0.1**
Leaf area index (m^2/m^2)	–0.4**	–0.4**	–0.4**	–0.4**
Stem area index (m^2/m^2)	–0.1**	–0.1**	–0.1**	–0.1**

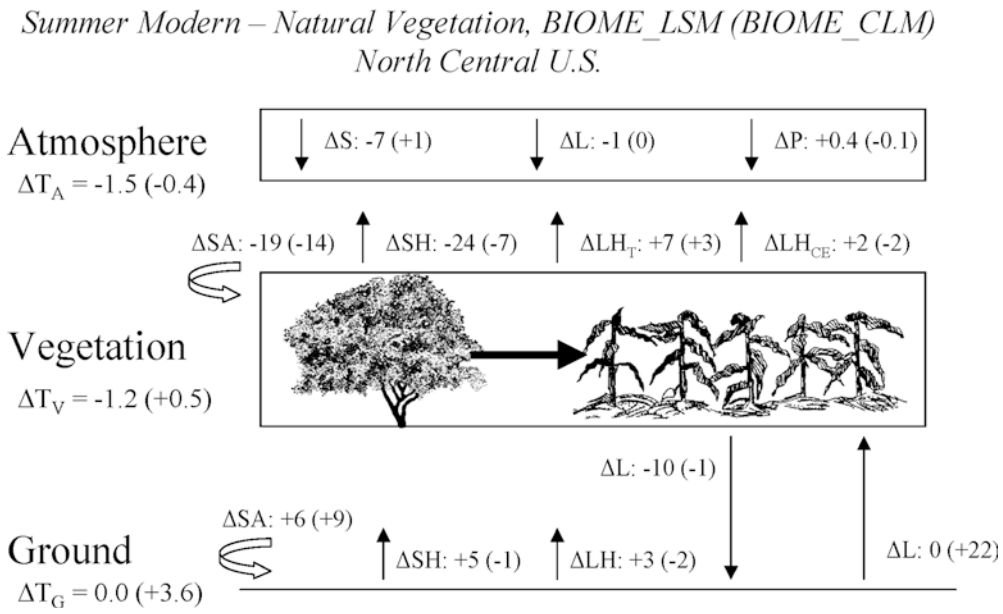

Fig. 5 Differences (modern minus natural vegetation) in summer (June, July, August) air (ΔT_A), vegetation (ΔT_V), and soil surface (ΔT_G) temperature (°C), and surface fluxes (*S*: solar radiation, *L*: longwave radiation, *SA*: absorbed solar radiation, *SH*: sensible heat flux, LH_T: transpiration, LH_{CE}: canopy evaporation, *LH*: ground evaporation (all in W/m^2), *P*: precipitation (mm/Day)) for the BIOME_LSM and BIOME_CLM experiments in the North Central region of the USA. Temperatures and surface fluxes for BIOME_CLM are in parentheses. The longwave radiation from vegetation to ground is calculated as $\varepsilon_V \sigma T_V^4$, where $\varepsilon_V = 1 - \exp[-(LAI + SAI)]$is the vegetation emissivity, σ = 5.67e – 8 is the Stefan-Boltzmann constant, and T_v is the vegetation temperature. The longwave from ground to vegetation is calculated as $\varepsilon_G \sigma T_G^4$, where ε_G = 0.96 is the ground emissivity and T_G is the ground temperature

soil surface temperature also cooled dramatically compared to BIOME_CLM, which reduced the longwave radiation from ground to canopy. Statistically significant cooling of 0.6 °C and 1.1 °C was also found for the Northeast and South regions, respectively (data not shown). This compares with cooling of 0.5 °C and 0.9 °C in BIOME_LSM.

These results indicate that the conclusion that modern vegetation cools USA mean summer climate does not appear to be as robust in the context of a warmer and drier land-surface model. However, the associated reduction in diurnal temperature range does appear to be relatively robust, particularly in summer in regions with the largest land-cover change.

Table 9 Differences (modern minus natural vegetation) in summer surface climatology using biome–derived datasets, and LSM1 as the land model (BIOME_LSM), CLM2 as the land model (BIOME_CLM), and with modifications to CLM2 parametrisations for transpiration and aerodynamic resistance (BIOME_CLM_TR) for the North Central (37–50°N, 100–85°W) region of the USA

Variable	BIOME_LSM	BIOME_CLM	BIOME_CLM_TR
Air temperature (°C)	–1.5**	–0.4	–1.2**
Soil surface temperature (°C)	0.0	3.6**	0.0
Precipitation (mm/day)	0.4**	–0.1	0.2
Sensible heat (W/m^2)	–18.5**	–8.0**	–12.8**
Latent heat (W/m^2)	12.0**	–1.6	7.7*
Canopy evaporation	2.1**	–2.0*	–0.6
Transpiration	6.5**	2.6*	5.3**
Ground evaporation	3.4*	–2.1**	3.0**
Btran (–)	0.2**	0.1	0.2

*$P < 0.10$, **$P < 0.05$

3.5 Impact of land-cover change datasets and model biogeophysics

Here, we briefly compare SAT_CLM with BIOME_LSM to address the combined impact of different model physics and improved surface datasets. In the SAT_CLM experiment, modern vegetation generally cools climate over much of the USA in all seasons (Fig. 3c). The cooling is statistically significant in winter in the North Central region and in spring and summer in the South region (Fig. 4). There was a significant reduction in diurnal temperature range of about 0.5–1.0 °C in the North Central and South regions in summer and autumn (Table 4).

The strong cooling in winter in SAT_CLM near the Great Lakes (Fig. 3c) is likely related to increased snowfall that increased albedo, reduced absorbed solar radiation, and cooled the surface. Decreases in exposed leaf and stem area also contributed to increased albedo

by exposing more of the snow-covered ground. In the North Central region for example, leaf and stem area decreased by 0.5 m^2/m^2, precipitation increased by 0.2 mm/day, snow depth increased by 3 cm, and albedo increased by 4% absolute, resulting in a decrease in air temperature of 1.3 °C. These changes are statistically significant at the 95% confidence level (data not shown).

SAT_CLM is significantly warmer than BIOME_LSM in summer and autumn in the North Central region (Fig. 4). As discussed in Sect. 3.4, the biogeophysical parametrisations of CLM2 and the absence of positive atmospheric feedback acted to reduce the summer and autumn cooling shown in BIOME_LSM. Favorable atmospheric forcing appears to be lacking in the SAT_CLM experiment as well (e.g., Table 5). However, CLM2 appears to be less sensitive to surface datasets than LSM1. SAT_CLM is significantly different from BIOME_CLM only in the South region in summer (Fig. 4).

In the context of improved surface datasets and a different land model, modern human-caused land-cover change cools climate over much of the USA and reduces the diurnal temperature range. However, the signal in mean summer temperature is small enough compared to model variability that it is only statistically detectable in certain regions.

4 Summary and conclusions

Climate simulations were performed with the LSM1 and CLM2 land-surface models in conjunction with biome-derived and satellite-derived land-cover change datasets to examine the response of North American climate to land-cover change. A statistically significant cooling signal in summer mean air temperature (–1.5 °C) and a reduction in the diurnal temperature range (–1.8 °C) was found for the north central USA using LSM1 and biome-derived datasets. This result indicates the conclusions of Bonan (1997, 1999) that the USA human-impacted landscape cools summer climate and reduces the diurnal temperature range are robust when a different atmospheric model is used.

The use of more realistic satellite-derived land-cover change datasets in LSM1 diminished the magnitude and spatial extent of the cooling signal in summer compared to biome-derived datasets. In the region with the most extensive land-cover change, the cooling signal was reduced to –1 °C. The reduction in diurnal temperature range changed to –1.3 °C. However, the changes in mean temperature and reduction in diurnal temperature range were still statistically significant ($P < 0.05$). The diminished cooling signal is partly due to the fact that the satellite-derived land-cover change is from a grass/tree mixture to crop while the biome-derived change is primarily forest to crop. The model ecological properties associated with crops are more similar to grasses than to trees. The intensity of agriculture in the satellite-derived modern vegetation dataset is also somewhat less than in the biome-derived dataset.

The use of a comparatively warmer and drier land-surface model (CLM2) further reduced the magnitude of summer cooling caused by land-cover change. The cooling signal in daily mean temperature in the north central USA was –0.5 °C while the reduction in diurnal temperature range was –0.6 °C. An additional experiment using the biome-derived datasets showed that important model differences contributing to the diminished cooling signal were related to parametrisations and land-cover properties for transpiration and soil to canopy air conductance. The replacement of these parametrisations in CLM2 by the corresponding ones in LSM1 resulted in a cooling signal comparable to that produced by LSM1. The modified CLM2 produced higher latent heat, lower sensible heat, more precipitation, and wetter soils, which resulted in cooler temperatures.

These results are generally consistent with other studies that concluded that land-cover change in North America has caused a cooling in near surface air temperature (Matthews et al. 2003; Bounoua et al. 2002; Govindasamy et al. 2001; Betts 2001; Bonan 1997, 1999; Brovkin et al. 1999; Hansen et al. 1998). However, several of these studies attribute the cooling primarily to increases in winter and spring surface albedo in regions affected by snow (Bounoua et al. 2002; Betts 2001; Brovkin et al. 1999; Hansen et al. 1998). While statistically significant cooling in winter and spring is evident in some of our experiments, our results suggest that the season in which cooling is dominant may depend on surface datasets, model biogeophysics, and geographic region (Figure 4). In particular, the modeling of vegetation albedo in the presence of snow requires further research (Zhou et al. 2003).

The area of pasture in the USA has increased by 237 Mha from 1700 to 1990 (Goldewijk 2001). The present study does not include human-induced land-cover change from natural vegetation to pasture because the Ramankutty and Foley (1999) global croplands dataset includes cropland temporarily used for pasture but not permanent pasture. However, the expansion of pasture area has been mostly at the expense of grasslands (Ramankutty et al. 2001), which have similar biophysical properties. Further research is required to ascertain the role of land-cover change involving pasture.

Our results suggest that the cooling in daily mean temperature and reduction in diurnal temperature range associated with North American land-cover change is robust but the magnitude and hence detectibility of the cooling signal depends on surface datasets and land model biogeophysics. The adequacy of the datasets used to represent land-cover change and the model biogeophysics pertaining to the physiological and morphological differences in land-cover types need to be carefully considered to understand

and quantify the impacts of land-cover change on climate.

Acknowledgements The authors thank Richard Betts and an anonymous reviewer for comments that improved the manuscript. Navin Ramankutty and Jonathan Foley are thanked for providing the global croplands data. This work was supported by the NASA Land Cover Land Use Change program through a grant W-19,735. The National Center for Atmospheric Research is sponsored by the National Science Foundation.

References

Betts RA (2001) Biogeophysical impacts of land use on present-day climate: near-surface temperature change and radiative forcing. Atmos Sci Lett 1, DOI:10.1006/asle.2001.0023

Beven KJ, Kirkby MJ (1979) A physically based variable contributing area model of basin hydrology. Hydrol Sci Bull 24: 43–69

Bonan GB (1996) A Land Surface model (LSM version 1.0) for ecological, hydrological, and atmospheric studies: technical description and user's guide. NCAR Tech Note NCAR/TN-417+STR, pp 150

Bonan GB (1997) Effects of land use on the climate of the United States. Clim Change 37: 449–486

Bonan GB (1998) The land surface climatology of the NCAR Land Surface Model coupled to the NCAR community climate model. J Clim 11: 1307–1326

Bonan GB (1999) Frost followed the plow: Impacts of deforestation on the climate of the United States. Ecol Appl 9: 1305–1315

Bonan GB (2001) Observational evidence for reduction of daily maximum temperature by croplands in the Midwest United States. J Clim 14: 2430–2442

Bonan GB, Oleson KW, Vertenstein M, Levis S, Zeng X, Dai Y, Dickinson RE, Yang Z-L (2002a) The land surface climatology of the Community Land Model coupled to the NCAR Community Climate Model. J Clim 15: 3123–3149

Bonan GB, Levis S, Kergoat L, Oleson KW (2002b) Landscapes as patches of plant functional types: an integrating concept for climate and ecosystem models. Global Biogeochem Cycles 16: DOI 10.1029/2000GB001360

Bounoua L, DeFries R, Collatz GJ, Sellers P, Khan H (2002) Effects of land cover conversion on surface climate. Clim Change 52: 29–64

Brovkin V, Ganopolski A, Claussen M, Kubatzki C, Petoukhov V (1999) Modelling climate response to historical land cover change. Glob Ecol Biogeogr 8: 509–517

Collins WD and co-authors (2003) Description of the NCAR Community Atmosphere Model (CAM2). Available at http://www.ccsm.ucar.edu/models/atm-cam/index.html

Dorman JL, Sellers PJ (1989) A global climatology of albedo, roughness length and stomatal resistance for atmospheric general circulation models as represented by the Simple Biosphere Model (SiB). J Appl Meteorol 28: 834–855

Goldewijk KK (2001) Estimating global land use change over the past 300 years: The HYDE database. Global Biogeochem. Cycles 15: 417–433

Govindasamy B, Duffy PB, Caldeira K (2001) Land use changes and Northern Hemisphere cooling. Geophys Res Lett 28: 291–294

Hansen JE, Sato M, Lacis A, Ruedy R, Tegen I, Mathews E (1998) Climate forcings in the Industrial era. Proc Natl Acad Sci 95: 12,753–12,758

Matthews HD, Weaver AJ, Eby M, Meissner KJ (2003) Radiative forcing of climate by historical land cover change. Geophys Res Lett 30: DOI 10.1029/2002GL016098

Ramankutty N, Foley JA (1999) Estimating historical changes in global land cover: croplands from 1700 to 1992. Global Biogeochem Cycles 13: 997–1027

Ramankutty N, Goldewijk KK, Leemans R, Foley J, Oldfield F (2001) Land cover change over the last three centuries due to human activities. Global Change Newsl 47: 17–19

Zhou L, Dickinson RE, Tian Y, Zeng X, Dai Y, Yang Z-L, Schaaf CB, Gao F, Jin Y, Strahler A, Myneni RB, Yu H,, Wu W, Shaikh M (2003) Comparison of seasonal and spatial variations of albedos from Moderate-Resolution Imaging Spectroradiometer (MODIS) and Common Land Model. J Geophys Res 108: DOI 10.1029/2002JD003326